SCIENCE CHINA Materials ARTICLES

mater.scichina.com link.springer.com

Published online 8 November 2019 | https://doi.org/10.1007/s40843-019-1203-0

Sci China Mater 2020, 63(3): 347–355

Facile synthesis of nickel cobalt selenide hollow nanospheres as efficient bifunctional electrocatalyst for rechargeable Zn-air battery

Xuerong Zheng[1,2], Jinfeng Zhang[1], Jihui Wang[1], Zhijia Zhang[3], Wenbin Hu[1] and Yajing Han[1*]

ABSTRACT **Designing high active, low cost and bifunctional electrocatalysts is urgent for developing clean energy storage and conversion systems. Transition metal selenides exhibit optimal electronic conductivity and tunable physicochemical properties, which endow them with potential for efficient electrocatalysts to facilitate the oxygen reduction and oxygen evolution reactions (ORR and OER). Herein, hollow $Ni_xCo_{0.85-x}Se$ nanospheres were synthesized using a facile polyol based solution chemical method. The $Ni_xCo_{0.85-x}Se$ exhibits an onset overpotential of 0.89 V for ORR, and an overpotential of 305 mV to achieve 10 mA cm^{-2} for OER. Moreover, the $Ni_xCo_{0.85-x}Se$ based Zn-air battery displays remarkable specific capacity and durability. Such superior catalytic performances can be attributed to the synergistic effect, large specific surface area and enhanced electron transfer rate. This approach provides a new way to design highly efficient bifunctional electrocatalysts for electrochemical energy storage and utilization.**

Keywords: transition metal selenides, bifunctional electrocatalyst, oxygen reduction reaction, oxygen evolution reaction, rechargeable Zn-air battery

INTRODUCTION

With the rapid increase of utilization of fossil fuels, environmental pollution is becoming one of the most serious global issues in recent years. It is urgent to develop green, low-cost, and high-efficiency clean energy storage and conversion system [1–5]. Zn-air batteries have attracted much attention due to their high theoretical energy density, safety and sustainability, and great efforts for improving the cycle stability and efficiency have been made [6–9]. However, the bottleneck of Zn-air batteries is developing efficient bifunctional electrocatalysts to promote the kinetics of oxygen evolution reaction (OER) and oxygen reduction reaction (ORR), which are the core of Zn-air batteries [10–13]. Up to now, the most efficient electrocatalysts are noble metal based catalysts, such as Pt, Ir, Ru and their alloys [14–16]. However, their earth scarcity, poor stability and high cost greatly limit their widespread application [17–19]. Moreover, the noble metal based catalysts cannot catalyze the ORR and OER simultaneously [20–22]. Therefore, exploring low-cost, highly efficient and bifunctional electrocatalysts is highly desired for Zn-air batteries.

As promising candidates to replace noble metal electrocatalysts, transition metal compounds, especially the transition metal selenides (TMSe) have attracted extensive attention owing to their high electric conductivity, large range of stoichiometric adjustability, and the corresponding diversified physicochemical properties [23–27]. For example, nickel selenides can form single phases of $NiSe_2$, Ni_3Se_4, Ni_6Se_5, NiSe, Ni_3Se_2, and $Ni_{0.95}Se$, which possess distinct crystal structures and thus exhibit different electronic, optic and magnetic properties [28–30]. As reported, several methods such as hydrothermal, physical vapor deposition and electrodeposition, have been applied to synthesize TMSe with controllable morphologies, such as nanosheets, nanoparticles, and nanoflowers [31–34]. For the utilization of TMSe in the electrocatalytic field, the electrocatalysts are mainly modified by the following strategies: (i) compositing the

[1] School of Materials Science and Engineering, Key Laboratory of Advanced Ceramics and Machining Technology of the Ministry of Education, Tianjin University, Tianjin 300072, China
[2] Department of Chemistry, Virginia Tech, Blacksburg, Virginia 24061, USA
[3] School of Materials Science and Engineering, Tianjin Polytechnic University, Tianjin 300387, China
* Corresponding author (email: hanyajing@tju.edu.cn)

catalysts with well conductive substrates, such as carbon nanotubes and graphene, to enhance the electronic conductivity; (ii) engineering micro-nanostructures to enlarge the exposed surface area; (iii) heteroatoms doping in the lattice structure [29–32]. However, it is still a great challenge to prepare pure phase of TMSe because of their variable crystal structures and atomic ratios. Moreover, due to the limited catalytic active sites exposure, the bifunctional electrocatalytic properties of TMSe should be further enhanced [35–39].

Herein, a facile and environment-friendly polyol solution chemical process was developed to synthesize pure phase of TMSe compounds. In this work, $Ni_xCo_{0.85-x}Se$ hollow nanosphere (NCS-HN) catalyst was synthesized under an ambient pressure, with triethylene glycol (TEG) as base solution, polyvinylpyrrolidone (PVP) as capping agent, nickel/cobalt nitrate as cationic precursors and selenium powder as ionic precursor. Benefiting from the larger specific surface area and smaller electrochemical impedance spectra (EIS), the NCS-HN displays much better ORR (305 mV for 10 mA cm^{-2}) and OER (0.89 V for onset overpotential) properties compared with the counterparts $Ni_{0.85}Se$ and $Co_{0.85}Se$. Moreover, the rechargeable Zn-air battery using NCS-HN as air electrode shows remarkable specific capacity of 718 mA h g^{-1} and has no obvious fading even after 80 h. Therefore, this work opens a new way to construct TM-based efficient bifunctional electrocatalysts for energy storage and conversion.

EXPERIMENTAL SECTION

Materials synthesis

$Ni_xCo_{0.85-x}Se$, $Ni_{0.85}Se$ and $Co_{0.85}Se$ were prepared by a facile polyol solution chemical process. Typically, for the synthesis of $Ni_xCo_{0.85-x}Se$, 0.5 mmol $Ni(NO_3)_2{\cdot}6H_2O$ and 0.5 mmol $Co(NO_3)_2{\cdot}6H_2O$ were dissolved in 10 mL TEG solution as cationic precursor at room temperature. 2.0 mmol Se powder and 0.01 g PVP were completely dissolved into 40 mL TEG solution in a three-neck flask equipped with a condenser as anionic precursor. The anionic solution was protected under nitrogen atmosphere. Then, the flask was heated up to 270°C under continuous stirring. The cationic precursor was injected into the hot solution in a short time and the color of the solution changed from transparent yellow to black, demonstrating the nucleation and growth of the particles. The solution was refluxed for 30 min for Ostwald ripening to form homogeneous morphology, followed by ultrasonical wash using ethanol for at least thrice. The obtained powder was dried at 60°C for further characterization. The $Ni_{0.85}Se$ and $Co_{0.85}Se$ were prepared using $Ni(NO_3)_2{\cdot}6H_2O$ or $Co(NO_3)_2{\cdot}6H_2O$ as cationic precursor with no changing of other factors.

Materials characterization

X-ray diffractometer (XRD) was characterized at 40 kV and 40 mA using Bruker D8 Advance with a scan rate of 4° min^{-1}. The morphology and microstructure of the products were analyzed using field emission scanning electron microscopy (FESEM, Hitachi 4800), transmission electron microscopy (TEM, jem-2100f, 200 kV) and high resolution TEM (HRTEM). Brunauer–Emmett–Teller (BET) specific surface areas were measured using Quantachrome instrument.

Electrocatalytic measurements

The ORR properties of the products were measured in O_2 saturated KOH solution (0.1 mol L^{-1}), and the OER properties were measured in N_2 saturated KOH solution (0.1 mol L^{-1}) using an IviumStat workstation under a standard three-electrode system at room temperature with the graphite rod, saturated calomel electrode (SCE), and the catalysts as counter electrode, reference electrode, and working electrode, respectively. For the preparation of electrode, the product (3 mg), carbon black (7 mg), isopropanol (965 μL) and 5 wt% Nafion solution (35 μL) were mixed and sonicated at least 30 min to form a homogeneous slurry. Then 150 μL of the slurry was dipped onto the two sides of the cleaned carbon clothes (1×1 cm^2) and dried at 60°C for 6 h. The coated carbon cloth can be used directly as electrode and the loading mass was about 0.6 mg cm^{-2}. The results reported in this paper were corrected with *iR* compensation and were transferred with reference to the reversible hydrogen electrode (RHE) based on the equation: $E_{vs.\ RHE} = E_{vs.\ SCE} + 1.067$ V. Before measuring the electrochemical performances of the catalysts, several cyclic voltammograms (CVs) curves were scanned at 100 and 20 mV s^{-1} to improve the wettability and hydrophilicity. The scan rates for OER and ORR characterization were 5 mV s^{-1}. Rotating ring-disk electrode (RRDE) results were performed using a rotating system (PHYCHEMI) by changing the speed from 400 to 2025 rpm connected to an electrochemical workstation. The electron transfer number (n) was calculated based on the following equation: $n = 4NI_d / (NI_d + I_r)$, where I_d is the disk current, I_r is the ring current and N is the current collection efficiency of the RRDE. The EIS were measured by changing the frequency from 10 kHz to 0.1 Hz.

Zn-air battery assembly

The rechargeable Zn-air battery was assembled with the prepared coated carbon cloth as the air cathode (1×1 cm^2), the mixture of KOH (6.0 mol L^{-1}) and $ZnCl_2$ (0.2 mol L^{-1}) as the electrolyte, and the Zn plate (1×2 cm^2) as the anode. The electrolyte (100 mL) was added into a beaker. The cathode and anode were fixed in the electrolyte and connected to the Land testing system, respectively. The electrolyte was O_2 saturated before testing. The charge/discharge performance, open circuit potential, cycling ability and specific capacity were measured using a LAND-CT2001A testing device at room temperature.

RESULTS AND DISCUSSION

The facile polyol solution chemical strategy was applied to prepare $Ni_xCo_{0.85-x}Se$ nanocrystals (Fig. 1). Se powder was added into the TEG base solution and heated to 270°C in a short time, close to the boiling temperature of TEG (285°C). As reported, the polyol molecules have two hydroxyl groups and can provide two hydrogen atoms and electrons when heated nearly to the boiling point, and thus exhibit relatively strong reductive ability to reduce Se into Se_2^{2-} [40–42]. The formation of the products can be divided into two sections: nucleation and growth. The burst nucleation of $Ni_xCo_{0.85-x}Se$ happened in a short time when the room-temperature cationic precursor was injected into the hot anionic solution. After that, the crystal nucleus grew into special morphology assisted by the surfactant PVP during refluxing. The morphology can be influenced by the factors such as synthetic temperature, additives, acidity and alkalinity. After refluxing and centrifugation, the catalyst slurry was coated onto the carbon clothes and dried for further utilizations.

The well-defined NCS-HNs were successfully prepared by the polyol solution chemical method, confirmed by series of structural and morphological characterizations. Fig. 2a shows the XRD pattern of $Ni_xCo_{0.85-x}Se$, in which the main diffraction peaks are between the peaks of standard $Ni_{0.85}Se$ and $Co_{0.85}Se$, indicating the successful preparation of $Ni_xCo_{0.85-x}Se$ using polyol solution chemical approach. The SEM image (Fig. 2b) shows that the diameters of $Ni_xCo_{0.85-x}Se$ nanospheres are about 100 nm and formed by the agglomeration of many small nanoparticles. Further, the TEM image (Fig. 2c) exhibits the hollow structure of $Ni_xCo_{0.85-x}Se$ nanospheres and the thickness of the shell is about 46 nm. The BET results (Fig. 2d) indicate that the $Ni_xCo_{0.85-x}Se$ possesses much higher specific surface area compared with the single phase of $Ni_{0.85}Se$ and $Co_{0.85}Se$, which may provide more catalytic sites for ORR and OER. Abundant heterointerfaces can be seen between two distinct nanoparticles, as indicated by the white lines in Fig. 2e, f, which was confirmed to be beneficial to enlarging the catalytic active sites and facilitating the electron transfer rate, thus improving the electrocatalytic performances. In addition, the lattice distance of 0.21 nm in the bulk or on the surface of hollow structure is corresponding to the (102) facet of $Ni_xCo_{0.85-x}Se$ nanocrystal (Fig. 2e, f). The X-ray photoelectron spectroscopy (XPS) was carried out for chemical state analyses on the surface of the $Ni_xCo_{0.85-x}Se$ (Fig. 2g–i). As shown in Fig. 2g, two peaks located at 854.7 and 873.5 eV are corresponding to Ni^{2+} in $Ni_xCo_{0.85-x}Se$. For Co 2p, the two peaks are located at 782.1 and 796.8 eV (Fig. 2h). The Se also displays a standard energy position at 53.7 eV (Fig. 2i). The elemental ratio of Ni:Co:Se is 0.41:0.44:1, measured by the XPS, demonstrating the successful preparation of

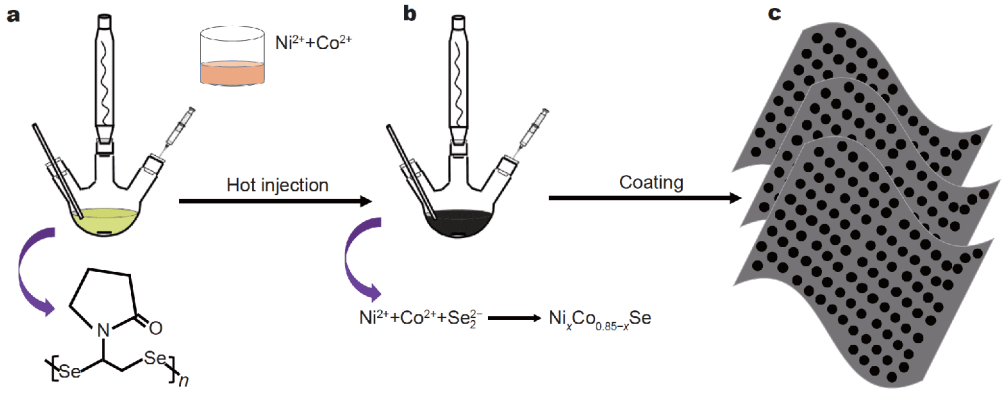

Figure 1 Schematic of preparing $Ni_xCo_{0.85-x}Se$ electrodes. (a) The Se precursor. (b) Hot injection and chemical reaction process. (c) Coating the $Ni_xCo_{0.85-x}Se$ onto the carbon clothes.

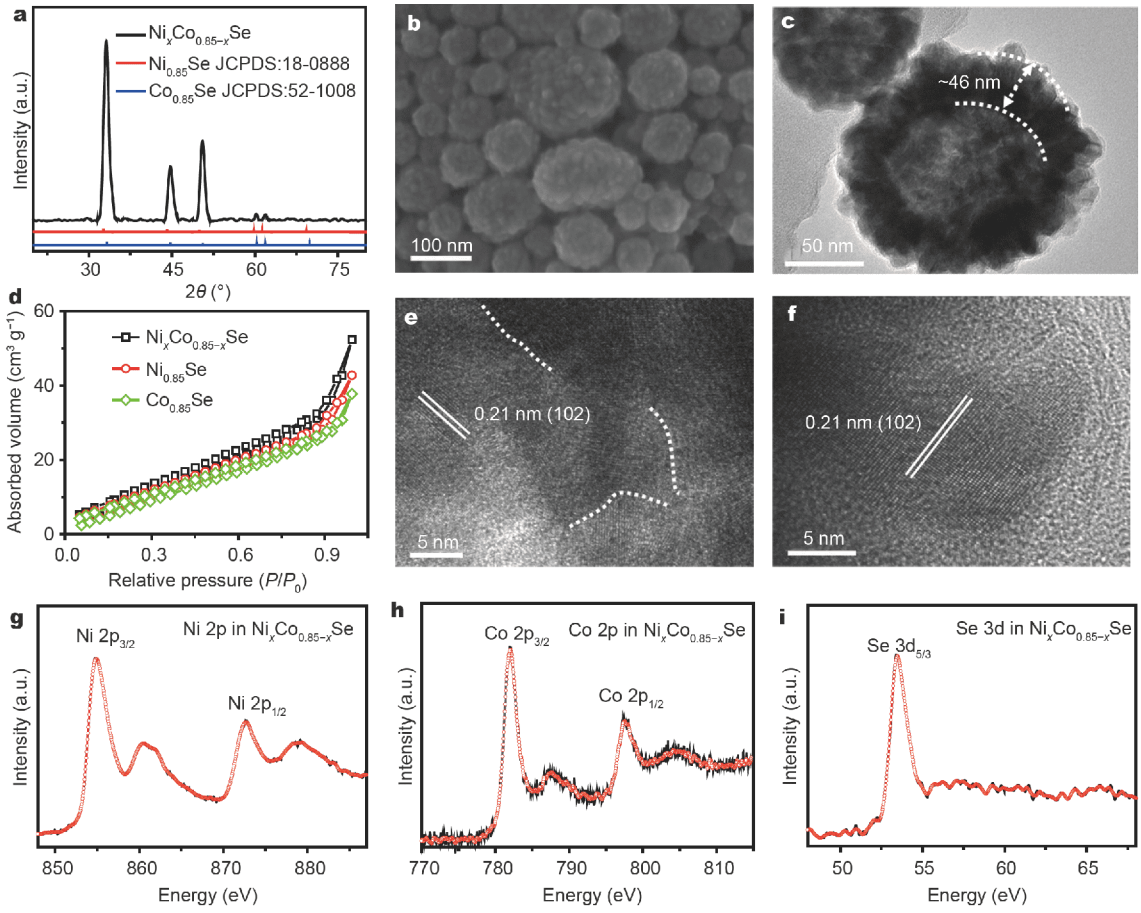

Figure 2 (a) XRD pattern of $Ni_xCo_{0.85-x}Se$ nanocrystals. (b) SEM and (c) TEM images of $Ni_xCo_{0.85-x}Se$. (d) The BET results of the catalysts $Ni_xCo_{0.85-x}Se$, $Co_{0.85}Se$ and $Ni_{0.85}Se$. (e, f) HRTEM images of $Ni_xCo_{0.85-x}Se$ nanocrystals synthesized by hot injection method. (g) Ni 2p, (h) Co 2p and (i) Se 3d XPS spectra.

$Ni_xCo_{0.85-x}Se$.

As expected, the $Ni_xCo_{0.85-x}Se$ catalyst exhibits better ORR performance compared with the counterparts of $Co_{0.85}Se$ and $Ni_{0.85}Se$. Fig. 3a shows the polarization curves of the $Ni_xCo_{0.85-x}Se$, $Co_{0.85}Se$ and $Ni_{0.85}Se$, which are compared with the commercial noble metal Pt/C (Table 1). The $Ni_xCo_{0.85-x}Se$ exhibits an onset overpotential of 0.89 V, 50 mV smaller than that of the Pt/C, but better than that of single phase $Co_{0.85}Se$ (0.86 V) and $Ni_{0.85}Se$ (0.84 V). The half-wave potential of $Ni_xCo_{0.85-x}Se$ (0.78 V) is also larger than that of $Co_{0.85}Se$ (0.74 V) and $Ni_{0.85}Se$ (0.73 V), indicating superior ORR kinetics of $Ni_xCo_{0.85-x}Se$ in the basic solution (Fig. 3b). Moreover, the RRDE measurement was performed to investigate the ORR catalysis mechanism (Fig. 3c). The diffusion limiting current density of $Ni_xCo_{0.85-x}Se$ proportionally increases with the increase of rotation speed, and reaches 5.28 mA cm^{-2} at 2025 rpm, indicating an efficient ORR process. In addition, the calculated Koutechy-Levich plots of $Ni_xCo_{0.85-x}Se$ are shown in Fig. 3d. Both the ORR linear sweep voltammetry (LSV) curves and the Koutechy-Levich plots of $Ni_xCo_{0.85-x}Se$ disclose a quite nearly quasi-4-electron ORR pathway (Fig. 3e), which is considered to be an efficient pathway for ORR catalysis. Moreover, the durability of $Ni_xCo_{0.85-x}Se$ in alkaline electrolyte was analyzed as shown in Fig. 3f. The electrode is stable for at least 10 h upon 0.8 V (*vs.* RHE), demonstrating the remarkable durability of $Ni_xCo_{0.85-x}Se$ for ORR process. Therefore, the above ORR electrochemical measurements suggest that $Ni_xCo_{0.85-x}Se$ can serve as a promising candidate for oxygen reduction process in electric devices.

To investigate the bifunctional feature of the electrocatalysts, the OER properties of $Ni_xCo_{0.85-x}Se$, $Co_{0.85}Se$ and $Ni_{0.85}Se$ were investigated in 0.1 mol L^{-1} KOH solution, and compared with commercial noble metal Ir/C. Fig. 4a shows the LSV curves of the products. The

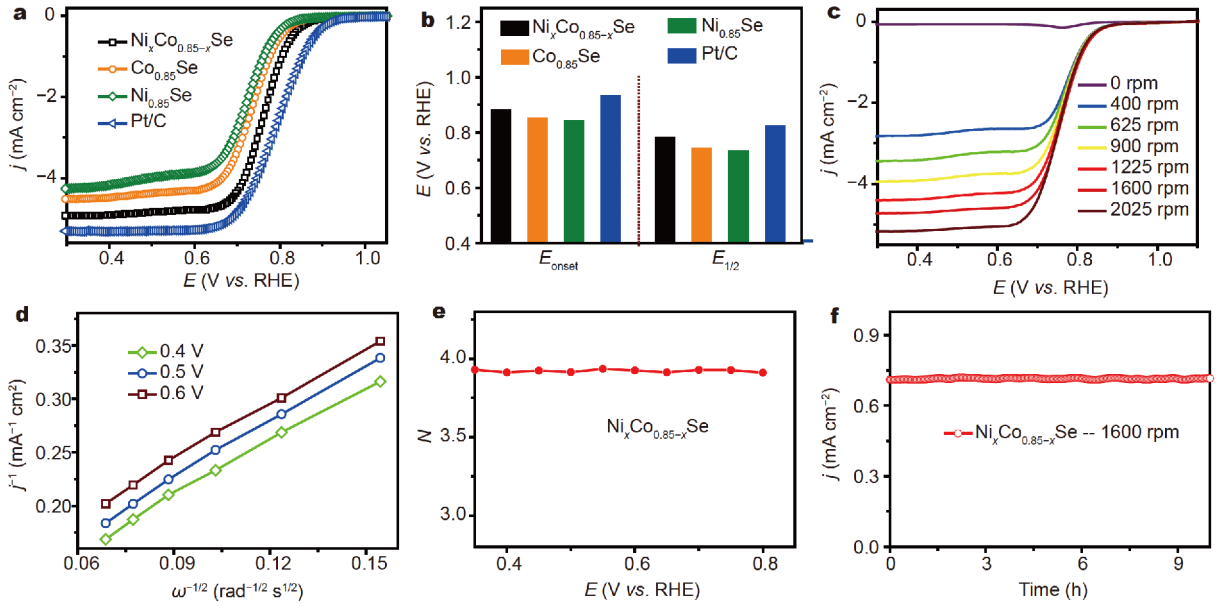

Figure 3 (a) The ORR LSV curves of $Ni_xCo_{0.85-x}Se$, $Co_{0.85}Se$, $Ni_{0.85}Se$ and Pt/C measured at a scan rate of 5 mV s^{-1} in 0.1 mol L^{-1} KOH solution. (b) The corresponding ORR onset and half overpotentials. (c) The ORR LSV curves of $Ni_xCo_{0.85-x}Se$ with different rotation speeds. (d) Koutechy-Levich plots of $Ni_xCo_{0.85-x}Se$ for ORR. (e) The calculated electron transfer number of $Ni_xCo_{0.85-x}Se$ for ORR. (f) The ORR stability performance of $Ni_xCo_{0.85-x}Se$ at 0.8 V.

overpotential of $Ni_xCo_{0.85-x}Se$ was 305 mV to achieve 10 mA cm^{-2}, about 105, 119 and 127 mV smaller than that of $Co_{0.85}Se$, $Ni_{0.85}Se$ and Ir/C, respectively (Table 1). This result is also comparable to other free standing TMSe catalysts reported recently [43–45]. Meanwhile, $Ni_xCo_{0.85-x}Se$ can achieve a current density of as high as 77 mA cm^{-2} at 500 mV, which is about 2.8 times better than that of $Co_{0.85}Se$ and $Ni_{0.85}Se$, indicating higher oxygen generation rate and prominent OER efficiency at relatively low overpotential. Moreover, the Tafel slope of $Ni_xCo_{0.85-x}Se$ (62 mV dec^{-1}) is much smaller than that of $Co_{0.85}Se$ (74 mV dec^{-1}), $Ni_{0.85}Se$ (78 mV dec^{-1}) and Ir/C (91 mV dec^{-1}), indicating higher OER kinetics of $Ni_xCo_{0.85-x}Se$. Fig. 4c shows the EIS Nyquist plots of the catalysts, demonstrating a similar trend with the Tafel slope results. Therefore, the above results verify that the better OER property of $Ni_xCo_{0.85-x}Se$ can be attributed to the enhanced electron transfer rate and higher catalytic kinetics. In addition, the operational durability is also an important criterion for the future commercialization. As shown in Fig. 4d, the LSV curves of $Ni_xCo_{0.85-x}Se$ repeated very well after 1 and 1000 CV cycles, indicating the impressive stability in basic solution. The chronoamperometric result (inset in Fig. 4d) also confirms the excellent stability of $Ni_xCo_{0.85-x}Se$, which increases only 0.016 V after more than 60 h.

Table 1 Summary of the electrochemical properties of the catalysts in this work

Catalysts	$V_{onset\text{-}ORR}$ (mV)	I_{ORR} (mA cm^{-2})	V_{OER} (mV) at 10 mA cm^{-2}	$Tafel_{OER}$ (mV dec^{-1})
$Ni_xCo_{0.85-x}Se$	0.89	4.9	305	62
$Ni_{0.85}Se$	0.84	4.3	424	78
$Co_{0.85}Se$	0.86	4.5	410	74
Pt/C	0.94	5.3	—	—
Ir/C	—	—	432	91

To analyze the microstructure evolution of $Ni_xCo_{0.85-x}Se$ after OER process, XRD, TEM and HRTEM characterizations were performed. Obviously, the crystallinity of $Ni_xCo_{0.85-x}Se$ decreased compared with that of pristine sample, indicating the change of phase structure after long-term OER process (Fig. 5a). However, the hollow structure of $Ni_xCo_{0.85-x}Se$ is stable without the morphology change after OER catalysis, demonstrating the stable microstructure of $Ni_xCo_{0.85-x}Se$ in basic solution (Fig. 5b). Furthermore, the lattice structure of $Ni_xCo_{0.85-x}Se$ becomes more obscure, suggesting that part of the microstructure turns to weak crystalline (Fig. 5c) or even amorphous (Fig. 5d). This phenomenon indicates that the oxides/hydroxides appear on the surface of the bulk after long-term OER process, where is verified to be

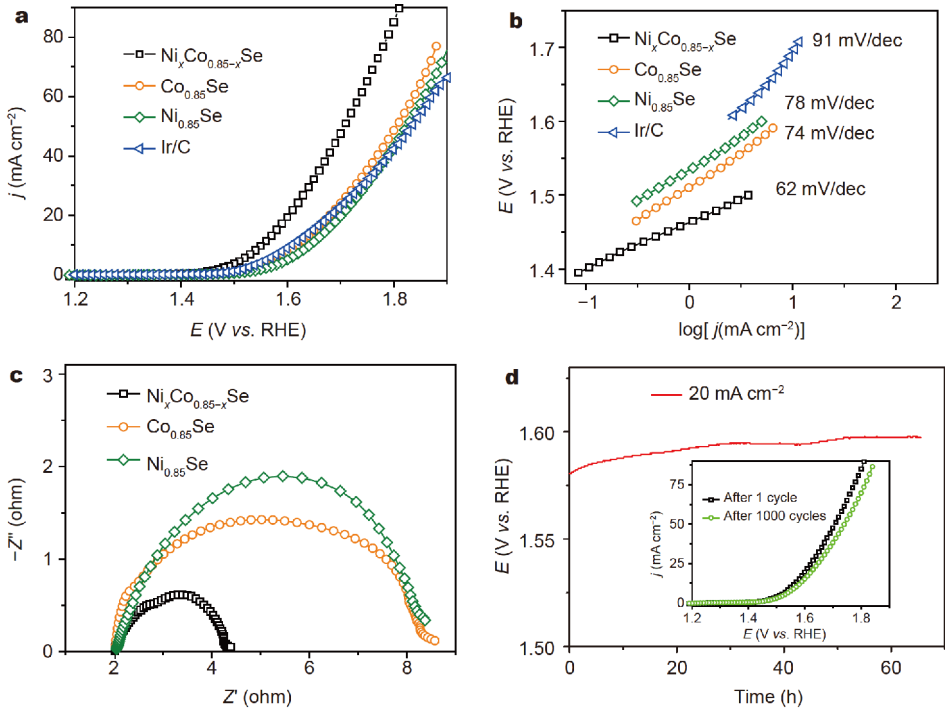

Figure 4 (a) The OER LSV curves of $Ni_xCo_{0.85-x}Se$, $Co_{0.85}Se$, $Ni_{0.85}Se$ and Ir/C measured at a scan rate of 5 mV s^{-1} in 0.1 mol L^{-1} KOH solution and (b) the corresponding Tafel slopes. (c) EIS results of $Ni_xCo_{0.85-x}Se$, $Co_{0.85}Se$ and $Ni_{0.85}Se$. (d) The chronoamperometric response of $Ni_xCo_{0.85-x}Se$. The inset is the LSV curves after different CV cycles.

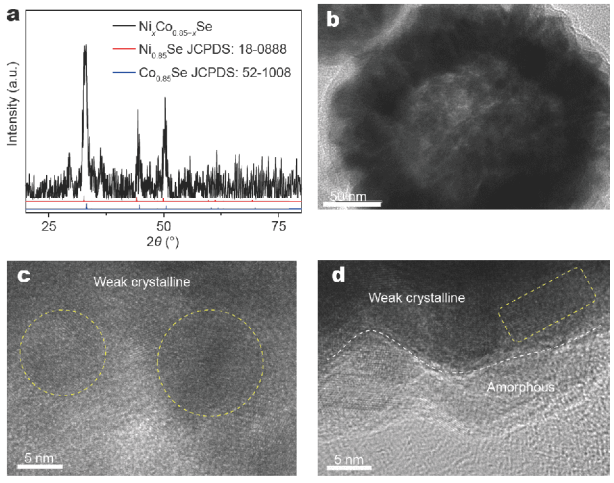

Figure 5 (a) XRD pattern, (b) TEM image and (c, d) HRTEM images of $Ni_xCo_{0.85-x}Se$ nanocrystals after OER process.

the true OER catalytic center, consistent with other related reports [46–48].

Generally, the overpotential difference (ΔE) between the OER (the overpotential at 10 mA cm^{-2}) and ORR (half-wave potential, $E_{1/2}$) demonstrates the performance of bifunctionality. Fig. 6b displays the ΔE values of the products. $Ni_xCo_{0.85-x}Se$ exhibits a ΔE value of 0.76 V, which is 110 and 150 mV smaller than that of $Co_{0.85}Se$ and $Ni_{0.85}Se$, respectively, suggesting that $Ni_xCo_{0.85-x}Se$ is a promising candidate for Zn-air battery. Encouraged by this result, $Ni_xCo_{0.85-x}Se$ was applied as air electrode in the rechargeable Zn-air battery system. The assembled Zn-air battery contains mainly three components: catalyst electrode as cathode, Zn foil as anode and the mixture of KOH and ZnCl as electrolyte, as schematically illustrated in Fig. 6a. To assess the property of the $Ni_xCo_{0.85-x}Se$-based Zn-air battery, charge/discharge curves were carried out and the corresponding power density was calculated, and compared with that of mixed Pt/C@Ir/C-based battery (Fig. 6c, d). Obviously, the $Ni_xCo_{0.85-x}Se$-based battery performance is better than that of the Pt/C@Ir/C. The $Ni_xCo_{0.85-x}Se$-based Zn-air battery delivers a specific capacity of 718 mA h g^{-1} at a current density of 10 mA cm^{-2}, normalized by the consumed weight of Zn foil (Fig. 6e, f). Moreover, the open circuit voltage of $Ni_xCo_{0.85-x}Se$-based Zn-air battery is as high as 1.37 V and maintains stable for at least 14 h, further confirming the stability of $Ni_xCo_{0.85-x}Se$ in the basic solution (inset in Fig. 6f). Additionally, the charge/discharge cycling performance of $Ni_xCo_{0.85-x}Se$-based Zn-air battery displays a

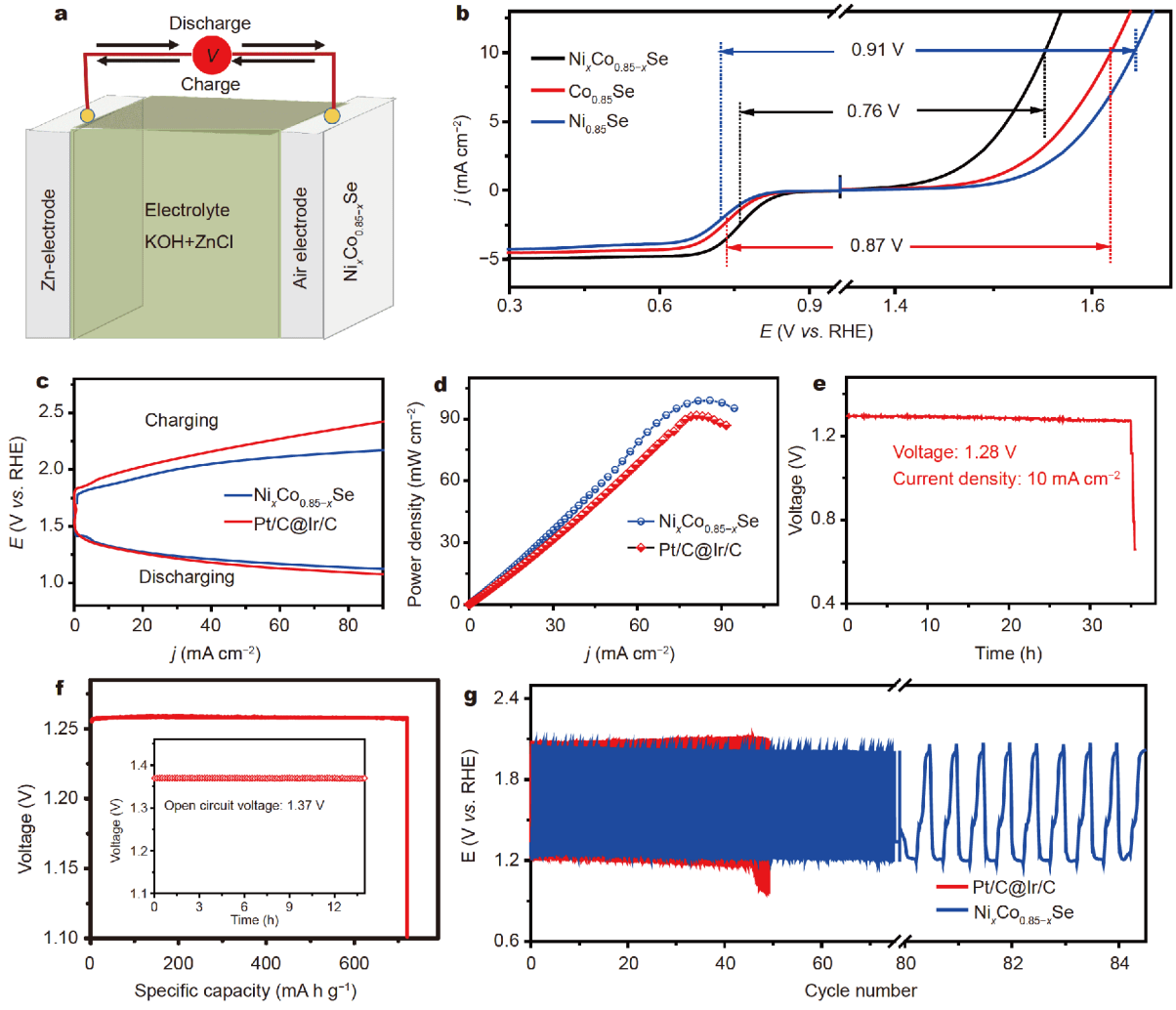

Figure 6 (a) Schematic of Zn-air battery. (b) ΔE calculated from the OER and ORR polarization curves of $Ni_xCo_{0.85-x}Se$, $Co_{0.85}Se$ and $Ni_{0.85}Se$. (c) The charge/discharge curves and (d) power density of $Ni_xCo_{0.85-x}Se$ and Pt/C@Ir/C based Zn-air batteries. (e) The galvanostatic discharge curves of the Zn-air battery with $Ni_xCo_{0.85-x}Se$ catalyst, normalized to the weight of the consumed zinc. (f) The specific capacity and open circuit voltage of $Ni_xCo_{0.85-x}Se$ based Zn-air battery, normalized by the consumed weight of zinc. (g) Galvanostatic charge/discharge cycling curves of Zn-air batteries with $Ni_xCo_{0.85-x}Se$ and Pt/C@Ir/C as catalysts.

voltage gap of ~0.87 V and a round-trip efficiency of 59%, with the charging voltage of ~2.05 V and discharging voltage of ~1.21 V, which is better than that of Pt/C@Ir/C-based battery (Fig. 6g). The above results demonstrate the superior rechargeability of $Ni_xCo_{0.85-x}Se$-based Zn-air battery. These results indicate that the $Ni_xCo_{0.85-x}Se$ deserves further investigation for the application in Zn-air batteries and other electronic devices.

CONCLUSION

In summary, we synthesized hollow structure $Ni_xCo_{0.85-x}Se$ nanospheres by using a facile polyol solution chemical method. For the preparation process, only ordinary utensils, polyol solution and relatively high temperature were used for the preparation of $Ni_xCo_{0.85-x}Se$ catalyst, which was low-cost, environmentally friendly and easy for large scale production. The prepared $Ni_xCo_{0.85-x}Se$ electrodes exhibit efficient bifunctional properties towards ORR and OER process, and much superior to the single phase of $Co_{0.85}Se$ and $Ni_{0.85}Se$. The optimal electrochemical performances of $Ni_xCo_{0.85-x}Se$ can be attributed to the enhanced specific surface area, electron conductivity and catalytic kinetics. In addition, the $Ni_xCo_{0.85-x}Se$ based Zn-air battery can deliver excellent specific capacity and long-term cycling stability. This work opens a new way for the preparation

of transition metal based bifunctional electrocatalysts in clean energy fields.

Received 22 July 2019; accepted 7 October 2019; published online 8 November 2019

1 Wang C, Xie NH, Zhang Y, *et al.* Silk-derived highly active oxygen electrocatalysts for flexible and rechargeable Zn–air batteries. Chem Mater, 2019, 31: 1023–1029

2 Liu Z, Zhang J, Hong T, *et al.* High-efficiency nanorod-nanosheet arrays sandwich photoelectrode for photoelectrochemical water splitting. Int J Hydrogen Energy, 2016, 41: 13359–13367

3 Hao Q, Chu Y, Zheng X, *et al.* Preparation of planar $CH_3NH_3PbI_3$ thin films with controlled size using 1-ethyl-2-pyrrolidone as solvent. J Alloys Compd, 2016, 671: 11–16

4 Zheng X, Cao Y, Han X, *et al.* Pt embedded Ni_3Se_2@NiOOH core-shell dendrite-like nanoarrays on nickel as bifunctional electrocatalysts for overall water splitting. Sci China Mater, 2019, 62: 1096–1104

5 Li H, Ji J, Zheng X, *et al.* Preparation of SnS quantum dots for solar cells application by an *in-situ* solution chemical reaction process. Mater Sci Semiconductor Processing, 2015, 36: 65–70

6 Dutta S, Indra A, Feng Y, *et al.* Self-supported nickel iron layered double hydroxide-nickel selenide electrocatalyst for superior water splitting activity. ACS Appl Mater Interfaces, 2017, 9: 33766–33774

7 Tian J, Liu Q, Asiri AM, *et al.* Self-supported nanoporous cobalt phosphide nanowire arrays: An efficient 3D hydrogen-evolving cathode over the wide range of pH 0–14. J Am Chem Soc, 2014, 136: 7587–7590

8 Fu G, Liu Y, Chen Y, *et al.* Robust N-doped carbon aerogels strongly coupled with iron–cobalt particles as efficient bifunctional catalysts for rechargeable Zn–air batteries. Nanoscale, 2018, 10: 19937–19944

9 Zhang Z, Liu G, Cui X, *et al.* Crystal phase and architecture engineering of lotus-thalamus-shaped Pt-Ni anisotropic superstructures for highly efficient electrochemical hydrogen evolution. Adv Mater, 2018, 30: 1801741

10 Wang T, Nam G, Jin Y, *et al.* NiFe (oxy)hydroxides derived from NiFe disulfides as an efficient oxygen evolution catalyst for rechargeable Zn-air batteries: The effect of surface S residues. Adv Mater, 2018, 30: 1800757

11 Fu G, Cui Z, Chen Y, *et al.* Ni_3Fe-N doped carbon sheets as a bifunctional electrocatalyst for air cathodes. Adv Energy Mater, 2017, 7: 1601172

12 Han X, He G, He Y, *et al.* Engineering catalytic active sites on cobalt oxide surface for enhanced oxygen electrocatalysis. Adv Energy Mater, 2018, 8: 1702222

13 Li Y, Zhong C, Liu J, *et al.* Atomically thin mesoporous Co_3O_4 layers strongly coupled with N-rGO nanosheets as high-performance bifunctional catalysts for 1D knittable zinc-air batteries. Adv Mater, 2018, 30: 1703657

14 Chen Z, Zhao H, Zhang J, *et al.* IrNi nanoparticle-decorated flower-shaped $NiCo_2O_4$ nanostructures: controllable synthesis and enhanced electrochemical activity for oxygen evolution reaction. Sci China Mater, 2017, 60: 119–130

15 Zeng S, Tong X, Zhou S, *et al.* All-in-one bifunctional oxygen electrode films for flexible Zn-air batteries. Small, 2018, 14: 1803409

16 Han X, Cheng F, Zhang T, *et al.* Hydrogenated uniform Pt clusters supported on porous $CaMnO_3$ as a bifunctional electrocatalyst for enhanced oxygen reduction and evolution. Adv Mater, 2014, 26: 2047–2051

17 Wang HF, Tang C, Zhang Q. A review of precious-metal-free bifunctional oxygen electrocatalysts: Rational design and applications in Zn−air batteries. Adv Funct Mater, 2018, 28: 1803329

18 Amiinu IS, Liu X, Pu Z, *et al.* From 3D ZIF nanocrystals to Co-N_x/C nanorod array electrocatalysts for ORR, OER, and Zn-air batteries. Adv Funct Mater, 2018, 28: 1704638

19 Singh S, Jain S, Ps V, *et al.* Hydrogen: A sustainable fuel for future of the transport sector. Renew Sustain Energy Rev, 2015, 51: 623–633

20 Chen X, Liu B, Zhong C, *et al.* Ultrathin Co_3O_4 layers with large contact area on carbon fibers as high-performance electrode for flexible zinc-air battery integrated with flexible display. Adv Energy Mater, 2017, 7: 1700779

21 Lee Y, Suntivich J, May KJ, *et al.* Synthesis and activities of rutile IrO_2 and RuO_2 nanoparticles for oxygen evolution in acid and alkaline solutions. J Phys Chem Lett, 2012, 3: 399–404

22 Yin J, Li Y, Lv F, *et al.* Oxygen vacancies dominated NiS_2/CoS_2 interface porous nanowires for portable zn-air batteries driven water splitting devices. Adv Mater, 2017, 29: 1704681

23 Zheng X, Han X, Liu H, *et al.* Controllable synthesis of Ni_xSe ($0.5 \leq x \leq 1$) nanocrystals for efficient rechargeable zinc–air batteries and water splitting. ACS Appl Mater Interfaces, 2018, 10: 13675–13684

24 Liu Y, Cheng H, Lyu M, *et al.* Low overpotential in vacancy-rich ultrathin $CoSe_2$ nanosheets for water oxidation. J Am Chem Soc, 2014, 136: 15670–15675

25 Sivanantham A, Shanmugam S. Nickel selenide supported on nickel foam as an efficient and durable non-precious electrocatalyst for the alkaline water electrolysis. Appl Catal B-Environ, 2017, 203: 485–493

26 Anugop B, Prasanth S, Rithesh Raj D, *et al.* Role of Mn^{2+} concentration in the linear and nonlinear optical properties of $Ni_{1-x}Mn_xSe$ nanoparticles. Optical Mater, 2016, 62: 297–305

27 Lee CT, Peng JD, Li CT, *et al.* Ni_3Se_4 hollow architectures as catalytic materials for the counter electrodes of dye-sensitized solar cells. Nano Energy, 2014, 10: 201–211

28 Umeyama N, Tokumoto M, Yagi S, *et al.* Synthesis and magnetic properties of NiSe, NiTe, CoSe, and CoTe. Jpn J Appl Phys, 2012, 51: 053001

29 Zhang X, Zhen M, Bai J, *et al.* Efficient NiSe-Ni_3Se_2/graphene electrocatalyst in dye-sensitized solar cells: The role of hollow hybrid nanostructure. ACS Appl Mater Interfaces, 2016, 8: 17187–17193

30 Moloto N, Moloto MJ, Coville NJ, *et al.* Synthesis and characterization of nickel selenide nanoparticles: size and shape determining parameters. J Cryst Growth, 2011, 324: 41–52

31 Wu X, He D, Zhang H, *et al.* $Ni_{0.85}Se$ as an efficient non-noble bifunctional electrocatalyst for full water splitting. Int J Hydrogen Energy, 2016, 41: 10688–10694

32 Tian Y, Ruan Y, Zhang J, *et al.* Controllable growth of NiSe nanorod arrays *via* one-pot hydrothermal method for high areal-capacitance supercapacitors. Electrochim Acta, 2017, 250: 327–334

33 Wang Z, Li J, Tian X, *et al.* Porous nickel–iron selenide nanosheets as highly efficient electrocatalysts for oxygen evolution reaction. ACS Appl Mater Interfaces, 2016, 8: 19386–19392

34 Fang L, Li W, Guan Y, *et al.* Tuning unique peapod-like $Co(S_xSe_{1-x})_2$ nanoparticles for efficient overall water splitting. Adv Funct Mater, 2017, 27: 1701008
35 Swesi AT, Masud J, Nath M. Nickel selenide as a high-efficiency catalyst for oxygen evolution reaction. Energy Environ Sci, 2016, 9: 1771–1782
36 Fang Z, Peng L, Lv H, *et al.* Metallic transition metal selenide holey nanosheets for efficient oxygen evolution electrocatalysis. ACS Nano, 2017, 11: 9550–9557
37 Li H, Chen S, Lin H, *et al.* Nickel diselenide ultrathin nanowires decorated with amorphous nickel oxide nanoparticles for enhanced water splitting electrocatalysis. Small, 2017, 13: 1701487
38 Hu X, Chen Y, Zhang M, *et al.* Alveolate porous carbon aerogels supported Co_9S_8 derived from a novel hybrid hydrogel for bifunctional oxygen electrocatalysis. Carbon, 2019, 144: 557–566
39 Subbarao U, Marakatti VS, Amshumali MK, *et al.* Size and morphology controlled NiSe nanoparticles as efficient catalyst for the reduction reactions. J Solid State Chem, 2016, 244: 84–92
40 Zheng X, Jin Z, Liu H, *et al.* Phase-controllable synthesis of Cu_xS nanocrystals by an ambient pressure tetraethylene glycol solution process. Synth Met, 2013, 169: 25–32
41 Zheng X, Han X, Zhang Y, *et al.* Controllable synthesis of nickel sulfide nanocatalysts and their phase-dependent performance for overall water splitting. Nanoscale, 2019, 11: 5646–5654
42 Zheng X, Jin Z, Liu H, *et al.* Single-phase and well-dispersed $Cu_{1.75}S$ nanocrystals by ambient pressure diethylene glycol solution synthesis. Appl Surf Sci, 2012, 266: 39–45
43 Han X, Wu X, Zhong C, *et al.* $NiCo_2S_4$ nanocrystals anchored on nitrogen-doped carbon nanotubes as a highly efficient bifunctional electrocatalyst for rechargeable zinc-air batteries. Nano Energy, 2017, 31: 541–550
44 Li Y, Yin J, An L, *et al.* Metallic $CuCo_2S_4$ nanosheets of atomic thickness as efficient bifunctional electrocatalysts for portable, flexible Zn-air batteries. Nanoscale, 2018, 10: 6581–6588
45 Li Y, Zhou W, Dong J, *et al.* Interface engineered *in situ* anchoring of Co_9S_8 nanoparticles into a multiple doped carbon matrix: highly efficient zinc–air batteries. Nanoscale, 2018, 10: 2649–2657
46 Chang J, Xiao Y, Xiao M, *et al.* Surface oxidized cobalt-phosphide nanorods as an advanced oxygen evolution catalyst in alkaline solution. ACS Catal, 2015, 5: 6874–6878
47 Stern LA, Feng L, Song F, *et al.* Ni_2P as a Janus catalyst for water splitting: the oxygen evolution activity of Ni_2P nanoparticles. Energy Environ Sci, 2015, 8: 2347–2351
48 Zheng X, Zhang Y, Liu H, *et al. In situ* fabrication of heterostructure on nickel foam with tuned composition for enhancing water-splitting performance. Small, 2018, 14: 1803666

Acknowledgements This work was supported by the National Natural Science Foundation of China (51804216). Zheng X acknowledges a scholarship from the China Scholarship Council (CSC) (201806255078).

Author contributions Zheng X and Han Y designed and engineered the samples; Zhang J and Zhang Z performed the experiments; Han Y performed the characterizations of SEM, TEM and XRD; Zheng X, Wang J and Hu W helped analyze and discuss the data; Zheng X wrote the manuscript with support from Han Y.

Conflict of interest The authors declare no conflict of interest.

Xuerong Zheng is a PhD student in the School of Materials Science and Engineering at Tianjin University. His recent research interests focus on the development of electrochemical metallurgy methods for preparing micro/nanostructured materials for electrochemical and electrocatalysis applications.

Yajing Han is an associate professor in the School of Materials Science and Engineering, Tianjin University. Her expertise is in the SEM, TEM and XRD analyses. Her research interests include metal and metal oxide nanostructures for electrochemical and energy applications.

$Ni_xCo_{0.85-x}Se$中空纳米球的溶液化学法合成、双功能特性及锌空电池应用

郑学荣[1,2], 张金凤[1], 王吉会[1], 张志佳[3], 胡文彬[1], 韩雅静[1*]

摘要 合成高活性、低成本、双功能特性的电催化剂是目前发展新能源材料的重要任务. 过渡金属硒化物具有较高的电导特性、可调节的物理化学特性等, 成为了开发高效氧还原和氧析出催化剂的研究热点. 本文采用多元醇溶液化学法合成了具有较大比表面积的$Ni_xCo_{0.85-x}Se$中空纳米球. 该催化剂的ORR起始电位达到0.89 V, OER在10 mA cm^{-2}电流密度下的过电位达到305 mV. 以$Ni_xCo_{0.85-x}Se$中空纳米球为空气电极、锌片为阴极组成的锌空电池具有良好的比容量和循环稳定性. $Ni_xCo_{0.85-x}Se$中空纳米球优异的催化性能主要归因于较大的比表面积、Ni和Co的协同催化特性以及良好的导电性. 本文为设计高效的锌空电池催化剂提供了良好的理论基础和实验支持.

